ACS OMEGA

http://pubs.acs.org/journal/acsodf

Article

Trapping the Transition State in a [2,3]-Sigmatropic Rearrangement by Applying Pressure

Sourabh Kumar, Rahel Weiß, Felix Zeller, and Tim Neudecker*

Cite This: *ACS Omega* 2022, 7, 45208−45214

Read Online

ACCESS | Metrics & More | Article Recommendations | Supporting Information

ABSTRACT: Transition states are of central importance in chemistry. While they are, by definition, transient species, it has been shown before that it is possible to "trap" transition states by applying stretching forces. We here demonstrate that the task of transforming the transition state of a chemical reaction into a minimum on the potential energy surface can be achieved using hydrostatic pressure. We apply the computational extended hydrostatic compression force field (X-HCFF) approach to the educt of a [2,3]-sigmatropic rearrangement in both static and dynamic calculations and find that the five-membered cyclic transition state of this reaction becomes a minimum at pressures in the range between 100 and 150 GPa. Born−Oppenheimer molecular dynamics (BOMD) simulations suggest that slow decompression leads to a 70:30 mix of the product and the educt of the sigmatropic rearrangement. Our findings are discussed in terms of geometric parameters and electronic rearrangements throughout the reaction. To provide reference data for experimental investigations, we simulated the IR, Raman, and time-resolved UV/vis absorption spectra for the educt, transition state, and product. We speculate that the trapping of transition states by using pressure is generally possible if the transition state of a chemical reaction has a more condensed geometry than both the educt and the product, which paves the way for new ways of initiating chemical reactions.

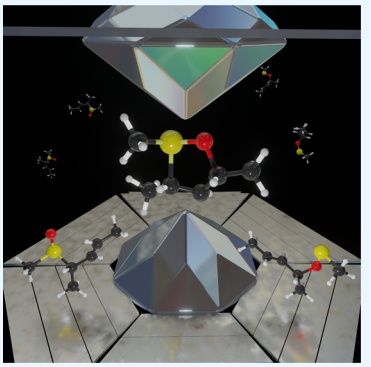

INTRODUCTION

The rearrangement of allylic sulfoxides to allylic sulfenate esters is a popular example of [2,3]-sigmatropic rearrangements.[1−3] This type of reaction is also known as the Mislow−Evans rearrangement[4−11] and is widely used in asymmetric synthesis due to the possibility of chirality transfer from the carbon bearing the sulfoxide group to the alcohol resulting from a subsequent reaction with an appropriate thiophile (Figure 1A). Hence, the Mislow−Evans rearrangement is a popular tool in the synthesis of bioactive substances and natural products like terpenes,[12] vernolepin,[13,14] amphidinol 3,[15] and pyrenolide D.[16]

The transition state of the Mislow−Evans rearrangement has attracted considerable attention because it determines the stereochemistry of the reaction.[17] It has been found that the Mislow−Evans rearrangement proceeds via a five-membered cyclic transition state (Figure 1A).[6,11,17−19] By using quantum chemical methods, we here demonstrate that the cyclic transition state of the Mislow−Evans rearrangement becomes a minimum under pressures between 100 and 150 GPa, which is a pressure range that is accessible with modern diamond-anvil cell technology.[20] While the "trapping" of the transition state of a chemical reaction has been achieved before with mechanical force,[21] to the best of our knowledge, this task has not yet been achieved with pressure. Our findings present a significant advancement over previous extrapolated data that suggest that the typically unstable cis-conformation of 1,2-dichloroethane can be stabilized by pressure,[22] and add to previous predictions concerning the evolution of transition states under pressure.[23] The possibility of transforming a transition state into a minimum on the potential energy surface paves the way for isolating and characterizing this transient chemical species and will more broadly open up new possibilities in chemical synthesis.

COMPUTATIONAL DETAILS

Several quantum chemical methods for the application of hydrostatic pressure to molecules during geometry optimizations have been reported.[23−30] In this paper, we used the extended hydrostatic compression force field (X-HCFF) approach[29] to apply pressure during geometry optimizations and Born−Oppenheimer molecular dynamics (BOMD) simulations, as implemented in the Q-Chem 5.4.2 program package,[31] since this method has been used successfully to predict structural parameters and chemical reactions in the GPa regime.[32] Density functional theory (DFT)[33,34] at the B3LYP[35−37]/6-31G(d)[38] level of theory was used as the electronic structure method, and 302 tessellation points per

Received: September 1, 2022
Accepted: November 10, 2022
Published: November 30, 2022

https://doi.org/10.1021/acsomega.2c05664
ACS Omega 2022, 7, 45208−45214

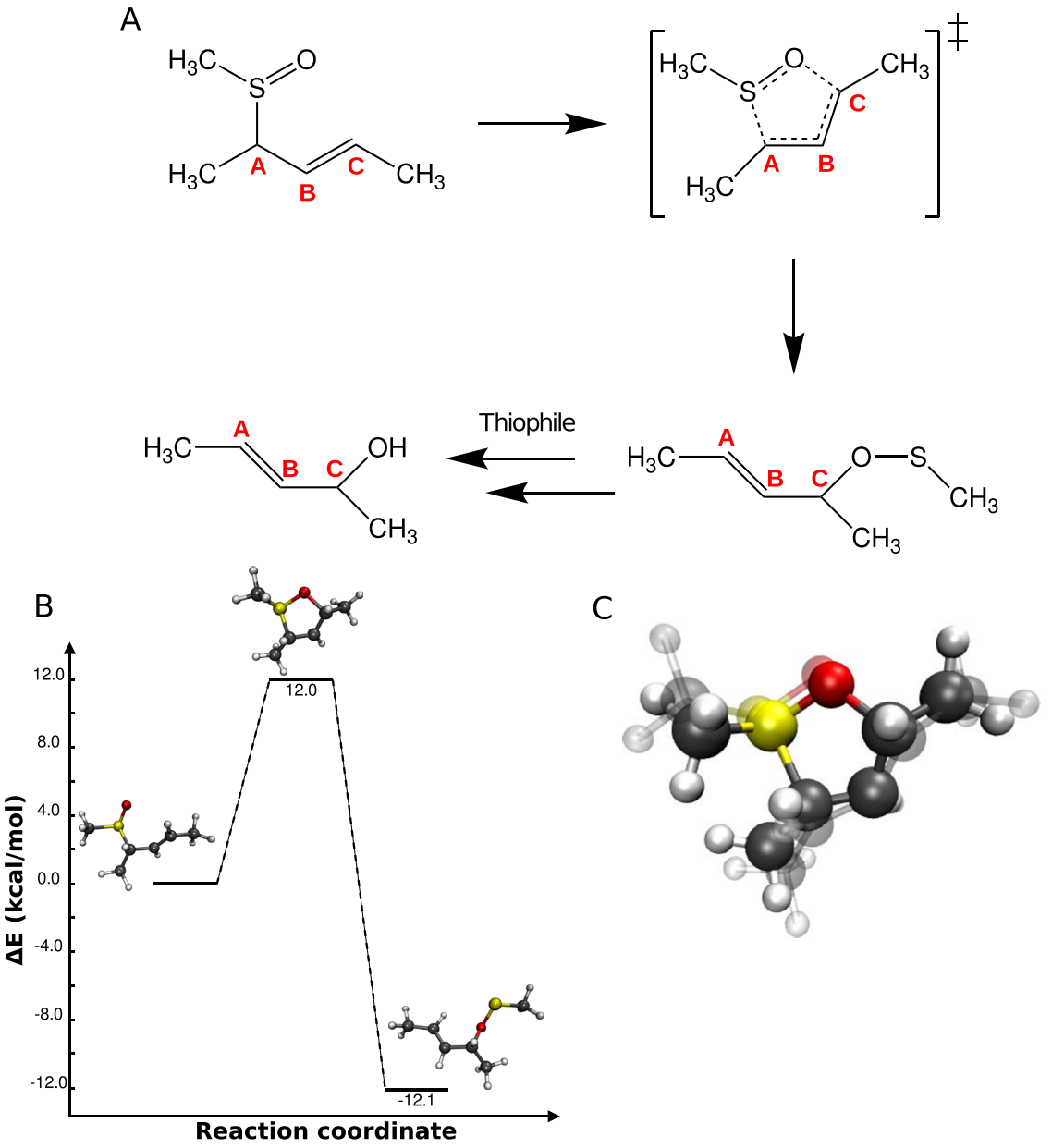

Figure 1. (A) Schematic representation, including labels of carbon atoms, and (B) energy profile of the Mislow−Evans rearrangement, calculated at the B3LYP/6-31G(d) level of theory. (C) Superimposed geometries of the structure found at 120 GPa (solid), calculated with the extended hydrostatic compression force field (X-HCFF), and the cyclic transition state of the Mislow−Evans rearrangement without pressure (transparent).

atom as well as a tessellation sphere scaling factor of 1.0 were used in the X-HCFF calculations. The choice of using this set of X-HCFF parameters was motivated in the original publication.[29] The nature of the transition state at P = 0 GPa was confirmed by the existence of a single imaginary frequency. Frequency analyses were carried out analytically at P = 0 GPa. At P > 0 GPa, frequency analyses of the structure found at 120 GPa were conducted by numerical differentiation (keyword ideriv 1) of the analytical X-HCFF gradient.

Ten individual BOMD simulations were run at a temperature of 300 K with an integration time step of 20 au. The optimized geometry of the educt of the Mislow−Evans rearrangement was taken as the initial geometry of all BOMD trajectories, and initial velocities were sampled randomly from a Maxwell−Boltzmann distribution. The simulations were conducted by increasing the pressure by 10 GPa every 96.8 fs until the average C_c−O distance in the current simulation window was lower than 1.5 Å, marking the formation of the five-membered ring. Depending on the trajectory, this was the case in the range between 100 and 150 GPa. Subsequently, decompression with the same rate was initiated until 0 GPa was reached.

Mayer bond orders[39,40] and electron densities at the bond critical points[41] were calculated with the Multiwfn 3.7 program package.[42] Q-Chem was used to generate the wave functions for these analyses. IR and Raman spectra were plotted using the IQmol program by applying a broadening with a default scaling factor of 1.

RESULTS AND DISCUSSION

While, according to our calculations, the cyclic transition state of the model Mislow−Evans reaction considered in this paper

https://doi.org/10.1021/acsomega.2c05664
ACS Omega 2022, 7, 45208−45214

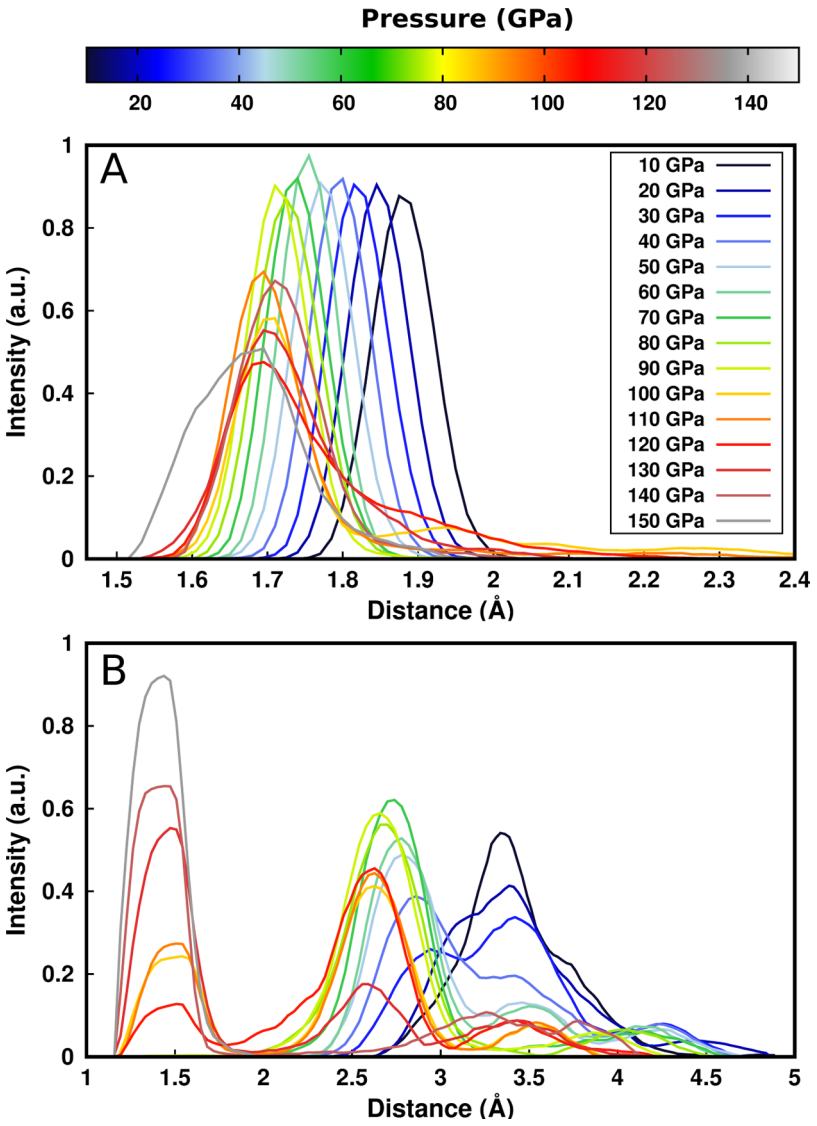

Figure 2. Normalized distances S−C_A (A) and C_c−O (B) for each individual 10 GPa simulation window averaged over all trajectories in the pressure range between 0 and 150 GPa.

(Figure 1B) lies 12.0 kcal mol^{-1} above the educt, geometry optimization with X-HCFF at a pressure of 120 GPa yields a five-membered cyclic structure (Figure 1C). This compressed geometry is remarkably close to the pressure-free transition state, with a mean root-mean-square deviation (RMSD) of only 0.3 Å between the ring atoms in the compressed and the pressure-free geometries (Table S1). While transition states have been found to disappear underpressure,[23] leading to the formation of the product of a chemical reaction with no further energy input, our calculations demonstrate that pressure can be used to transform a transition state into a minimum on the potential energy surface. The disappearance of imaginary frequencies of the obtained cyclic structure above 110 GPa (Figure S2) confirms this finding from a theoretical point of view.

It must be noted that the pressure required to form the cyclic structure depends quite heavily on the chosen density functional (Figure S1). While B3LYP/6-31G(d) yields an average pressure, this finding will motivate a more thorough benchmark of density functionals in future calculations of high-pressure properties.

Despite the intriguing notion that a transition state can be trapped by pressure, this finding is intuitive since the transition state of the Mislow−Evans rearrangement has a more condensed geometry than both the educt and the product. A preference for the transition-state geometry is therefore expected at elevated pressures.

To investigate the formation of the five-membered ring in the model Mislow−Evans reaction under pressure more closely, we conducted 10 individual BOMD simulations, in which we increased the pressure in increments of 10 GPa every 96.8 fs. Two representative distances, S−C_A and C_c−O (cf. Figure 1A for the labels), were averaged over all 10 simulations for each 10 GPa simulation window up to the maximum applied pressure. In agreement with chemical intuition, the S−C_A bond shortens with increasing pressure (Figure 2A). Up to approx. 90 GPa, the S−C_A bond length decreases fairly linearly with increasing pressure, and, since pressure is proportional to force, this observation shows that the compression of the S−C_A bond is a harmonic process throughout a remarkably large pressure range.

https://doi.org/10.1021/acsomega.2c05664
ACS Omega 2022, 7, 45208−45214

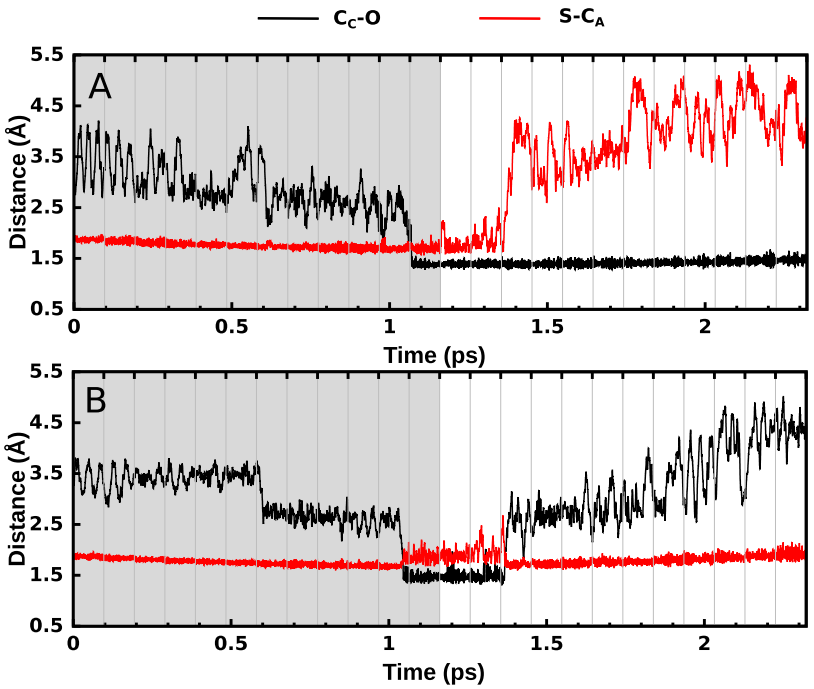

Figure 3. Time evolution of the distances C_c−O (black line) and S−C_A (red line) for two representative BOMD simulations of the model system under hydrostatic pressure in which the formation of the product (A) or of the educt (B) of the Mislow−Evans rearrangement is observed, respectively. Gray-shaded areas signify increasing compression, whereas white areas denote decompression. The pressure was changed by 10 GPa at each of the gray vertical lines.

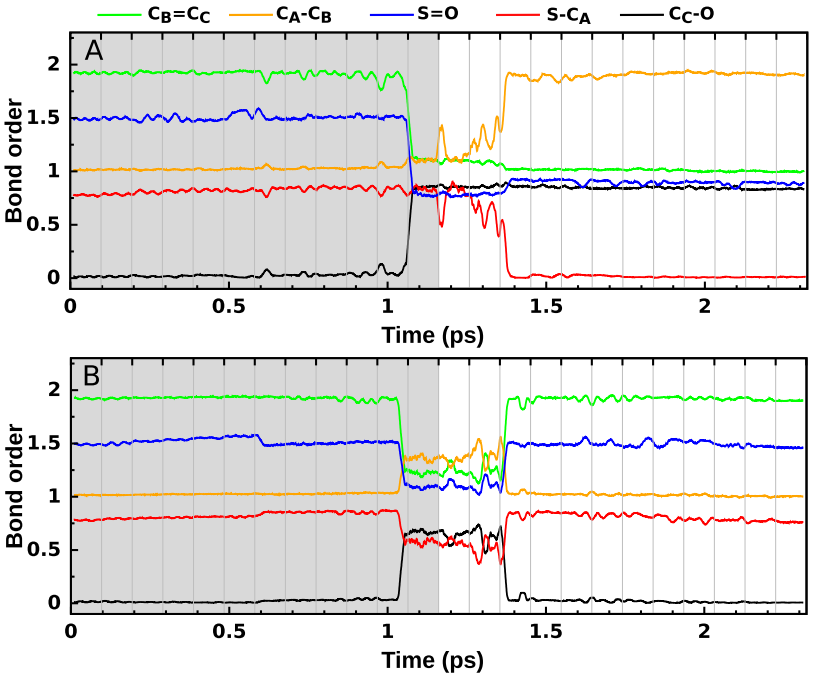

Figure 4. Time series plot of the Mayer bond orders of the bonds in the five-membered ring throughout two representative BOMD trajectories in which the product (A) or the educt (B) of the Mislow−Evans rearrangement is formed, respectively.

Turning to the C_c−O distance (Figure 2B), the distribution initially only broadens up to a pressure of 20 GPa since C_c and O are not bonded at first. An intermediate, slightly compressed geometry with a C_c−O distance between 2.5 and 3 Å is subsequently generated, followed by the gradual generation of cyclic species in which C_c and O are bonded, as evidenced by the accumulation of structures with a C_c−O distance of approx. 1.5 Å at pressures above 100 GPa.

The length of the C_c−O bond, which forms during the Mislow−Evans rearrangement, and the S−C_A bond, which breaks, are shown in Figure 3 as a function of time for two representative BOMD trajectories. In the first trajectory (Figure 3A), the formation of the five-membered ring can be observed at approx. 1.05 ps (120 GPa), marked by a sharp decrease in the C_c−O distance. Subsequently, slow decompression leads to the rupture of the S−C_A bond, yielding the

https://doi.org/10.1021/acsomega.2c05664
ACS Omega 2022, 7, 45208−45214

reaction product. While in the second trajectory (Figure 3B) the formation of the five-membered ring can be observed at a pressure of 120 GPa as well, decompression in this case leads to the recovery of the educt due to the rupture of the C_c-O bond and not the $S-C_A$ bond. Similar observations are made for other structural parameters involved in the formation of the five-membered ring (Figures S3 and S4).

The possibility to either form the product or to recover the educt is the expected behavior for a system that is held artificially at the transition state since it can move in either direction when the constraint is lifted, depending on the instantaneous nuclear velocities that are present upon decompression. In 7 out of the 10 simulations, the formation of the product is observed, whereas the educt is recovered in the remaining three simulations. This observation lends further evidence that a transition state was isolated using pressure. The pressure required to form the five-membered ring ranges between 100 and 150 GPa, depending on the trajectory. Details on each individual trajectory are given in the Supporting Information (Table S2).

The formation of the five-membered ring and its transformation to either the product or the educt of the Mislow–Evans rearrangement upon decompression can also be understood in terms of changes in Mayer bond orders[39,40] throughout the BOMD simulations (Figure 4). While the $C_B=C_c$ bond loses its double-bond character upon the formation of the five-membered ring, the bond order of the C_A-C_B bond increases, signifying an increase in double-bond character. In the trajectory in which the product of the Mislow–Evans reaction is formed upon decompression (Figure 4A), these changes are permanent. In addition, the bond order analysis reveals the rupture of the $S-C_A$ bond and the formation of the C_c-O bond, completing the rearrangement. Contrarily, the decrease in the $S-C_A$ bond order and the formation of the C_c-O bond are only transitory in the trajectory that recovers the educt upon decompression (Figure 4B). As soon as the five-membered ring dissociates upon decompression and the educt forms, the bond orders return to their initial values in this trajectory.

The formation of the product and the educt after the release of pressure in the BOMD trajectories can also be observed in the corresponding time-resolved UV/vis absorption spectra (Figure S5). Initially, peaks in the region between 200 and 220 nm are found. With the formation of the transition state at around 1.05 ps, the spectrum broadens and shifts toward longer wavelengths. When pressure is removed and the educt is formed, the peaks are shifted back to the region between 200 and 250 nm, whereas product formation leads to peaks between 200 and 280 nm.

Analogous effects can be observed in the propagation of electron densities at the bond critical points throughout the BOMD trajectories (Figure S6): in addition to an overall increase in electron density with increasing pressure, which is due to the compressed nuclear scaffold and the shortened bonds, shifts in electron density mark the formation of the five-membered cyclic structure at high pressure and its transformation to either the product or the educt of the Mislow–Evans rearrangement upon decompression.

A further method for a possible experimental characterization of the trapped transition state is IR and Raman spectroscopy (Figures S7 and S8). Upon the formation of the cyclic structure, the stretching modes of the methyl groups are shifted from an initial 3000–3300 to 3600–3900 cm^{-1}, a process that is accompanied by a decrease in IR intensities. The final generation of the product shifts these peaks back to the region of 3000–3200 cm^{-1}.

CONCLUSIONS

The static quantum chemical calculations and BOMD simulations presented in this study demonstrate that the five-membered cyclic transition state of a model Mislow–Evans rearrangement can be "trapped" by applying hydrostatic pressures in the range between 100 and 150 GPa. Decompression leads to the formation of the product of the rearrangement in 7 out of 10 trajectories, whereas the educt is recovered in the remaining three simulations. Our future studies will focus on the influence of environmental factors like chemical substitution[43] or the solvent in a multiscale simulation setup. We hope that our calculations spark an interest in experimental studies on the piezochemical isolation of transitory species in sigmatropic rearrangements and other chemical reactions. Calculated spectroscopic properties of the involved species that were presented here will provide reference data for such experimental studies. We speculate that transition states can generally be isolated using pressure if the transition-state geometries are more condensed than both the educt and the product of the reaction.

ASSOCIATED CONTENT

Supporting Information

The Supporting Information is available free of charge at https://pubs.acs.org/doi/10.1021/acsomega.2c05664.

Influence of functionals on the "trapping" pressure; structural parameters of five-membered ring; number of imaginary frequencies as a function of pressure; propagation of bond angles in the BOMD trajectories; time evolution of the RMSD; barochemical and structural data for the BOMD trajectories; time-resolved UV/vis spectra; propagation of electron densities in the BOMD simulations; and IR and Raman spectra (PDF)

AUTHOR INFORMATION

Corresponding Author

Tim Neudecker − *Institute for Physical and Theoretical Chemistry, University of Bremen, D-28359 Bremen, Germany; Bremen Center for Computational Materials Science, University of Bremen, D-28359 Bremen, Germany; MAPEX Center for Materials and Processes, University of Bremen, D-28359 Bremen, Germany;* orcid.org/0000-0001-7599-3578; Email: neudecker@uni-bremen.de

Authors

Sourabh Kumar − *Institute for Physical and Theoretical Chemistry, University of Bremen, D-28359 Bremen, Germany;* orcid.org/0000-0002-1303-2920

Rahel Weiß − *Institute for Physical and Theoretical Chemistry, University of Bremen, D-28359 Bremen, Germany*

Felix Zeller − *Institute for Physical and Theoretical Chemistry, University of Bremen, D-28359 Bremen, Germany*

Complete contact information is available at: https://pubs.acs.org/10.1021/acsomega.2c05664

Notes

The authors declare no competing financial interest.

https://doi.org/10.1021/acsomega.2c05664
ACS Omega 2022, 7, 45208−45214

■ ACKNOWLEDGMENTS

The authors gratefully acknowledge the University of Bremen, the Bremen Center for Computational Materials Science (BCCMS), and the MAPEX Center for Materials and Processes for financial support and for providing computational resources.

■ REFERENCES

(1) Reggelin, M.[2,3]-sigmatropic rearrangements of allylic sulfur compounds. In *Sulfur-Mediated Rearrangements II*; Springer: Berlin, Heidelberg, 2007; Vol. *275*, pp 1−65.
(2) Tang, F.; Yao, Y.; Xu, Y.; Lu, C. Diastereoselective Aza-Mislow−Evans Rearrangement of N -Acyl tert -Butanesulfinamides into α-Sulfenyloxy Carboxamides. *Angew. Chem.* **2018**, *130*, 15809−15812.
(3) Colomer, I.; Velado, M.; Ferna de la Pradilla, R.; Viso, A. From Allylic Sulfoxides to Allylic Sulfenates: Fifty Years of a Never-Ending [2, 3]-Sigmatropic Rearrangement. *Chem. Rev.* **2017**, *117*, 14201−14243.
(4) Rayner, D. R.; Miller, E. G.; Bickart, P.; Gordon, A. J.; Mislow, K. Mechanisms of Thermal Racemization of Sulfoxides. *J. Am. Chem. Soc.* **1966**, *88*, 3138−3139.
(5) Miller, E. G.; Rayner, D. R.; Mislow, K. Thermal Rearrangement of Sulfenates to Sulfoxides1. *J. Am. Chem. Soc.* **1966**, *88*, 3139−3140.
(6) Bickart, P.; Carson, F. W.; Jacobus, J.; Miller, E. G.; Mislow, K. The Thermal Racemization of Allylic Sulfoxides and the Interconversion of Allylic Sulfoxides and Sulfenates. Mechanism and Stereochemistry1,2. *J. Am. Chem. Soc.* **1968**, *90*, 4869−4876.
(7) Evans, D. A.; Andrews, G. C.; Sims, C. L. Reversible 1,3 Transposition of Sulfoxide and Alcohol Functions. Potential Synthetic Utility. *J. Am Chem. Soc.* **1971**, *93*, 4956−4957.
(8) Evans, D. A.; Andrews, G. C. Nucleophilic Cleavage of Allylic Sulfenate Esters. Mechanistic Observations. *J. Am Chem. Soc.* **1972**, *94*, 3672−3674.
(9) Evans, D. A.; Andrews, G.; Fujfmoto, T. T.; Wells, D. Stereoselective Synthesis of Trisubstituted Olefins. *Tetrahedron Lett.* **1973**, *14*, 1389−1392.
(10) Evans, D. A.; Andrews, G. C.; Fujimoto, T. T.; Wells, D. The application of allylic sulfoxide anions as vinyl anion equivalents. A general synthesis of allylic alcohols. *Tetrahedron Lett.* **1973**, *14*, 1385−1388.
(11) Tang, R.; Mislow, K. Rates and Equilibria in the Interconversion of Allylic Sulfoxides and Sulfenates. *J. Am Chem. Soc.* **1970**, *92*, 2100−2104.
(12) Masaki, Y.; Hashirnoto, K.; Sakuma, K.; Kaji, K. Facile Regio- and Stereo-specific Allylic Oxidation of gem-Dimethyl Olefins via Addition of Benzenesulphenyl Chloride. Synthesis of Allylic Oxygenated Terpenes. *J. Chem. Soc., Perkin Trans. 1* **1984**, *1*, 1289−1295.
(13) Iio, H.; Isobe, M.; Kawai, T.; Goto, T. Total Synthesis of Vernolepin. 2.1 Stereocontrolled Synthesis of (±)-Vernolepin. *J. Am. Chem. Soc.* **1979**, *101*, 6076−6081.
(14) Zutterman, F.; De Wilde, H. D.; Mijngheer, R.; De Clercq, P. D.; Vandewalle, M. A total synthesis of (+-)-Vernolepin. *Tetrahedron* **1979**, *35*, 2389−2396.
(15) de Vicente, J.; Huckins, J. R.; Rychnovsky, S. D. Synthesis of the C31−C67 Fragment of Amphidinol 3. *Angew. Chem.* **2006**, *118*, 7416−7420.
(16) Engstrom, K. M.; Mendoza, M. R.; Navarro-villalobos, M.; Gin, D. Y. Total Synthesis of (+)-Pyrenolide D. *Angew. Chem., Int. Ed.* **2001**, *40*, 1128−1130.
(17) Hoffmann, R. W. Stereochemistry of [2,3]Sigmatropic Rearrangements. *Angew. Chem., Int. Ed.* **1979**, *18*, 563−572.
(18) Jones-Hertzog, D. K.; Jorgensen, W. L. Elucidation of Transition Structures and Solvent Effects for the Mislow — Evans Rearrangement of Allylic Sulfoxides. *J. Am Chem. Soc.* **1995**, *117*, 9077−9078.
(19) Freeman, F.; Bathala, R. M.; Cavillo, J. E.; Huang, A. C.; Jackson, T. K.; Lopez-Mercado, A. Z.; Phung, S.; Suh, J.; Valencia, J. Diego O. [2,3]-Sigmatropic Rearrangements of Hydrogen and Alkyl 3-Propenyl Sulfoxides: A Computational Study. *Int. J. Quantum Chem.* **2006**, *106*, 2390−2397.
(20) Li, M.; Zhang, Q.; Zhou, Y. N.; Zhu, S. Let spiropyran help polymers feel force! *Prog. Polym. Sci.* **2018**, *79*, 26−39.
(21) Lenhardt, J. M.; Ong, M. T.; Choe, R.; Evenhuis, C. R.; Martinez, T. J.; Craig, S. L. Trapping a diradical transition state by mechanochemical polymer extension. *Science* **2010**, *329*, 1057−1060.
(22) Takaya, H.; Taniguchi, Y.; Wong, P.; Whalley, E. Effect of pressure on molecular conformations. iii. internal rotation angle in gauche-1, 2-dichloroethane and gauche-1, 2-dibromoethane. *J. Chem. Phys.* **1981**, *75*, 4823−4828.
(23) Chen, B.; Hoffmann, R.; Cammi, R. The Effect of Pressure on Organic Reactions in Fluids—a New Theoretical Perspective. *Angew. Chem. Int. Ed.* **2017**, *56*, 11126−11142.
(24) Stauch, T. Quantum chemical modeling of molecules under pressure. *Int. J. Quantum Chem.* **2020**, *121*, No. e26208.
(25) Subramanian, G.; Mathew, N.; Leiding, J. A generalized force-modified potential energy surface for mechanochemical simulations. *J. Chem. Phys.* **2015**, *143*, No. 134109.
(26) Stauch, T.; Chakraborty, R.; Head-Gordon, M. Quantum Chemical Modeling of Pressure-Induced Spin Crossover in Octahedral Metal-Ligand Complexes. *ChemPhysChem* **2019**, *20*, 2742−2747.
(27) Cammi, R.; Verdolino, V.; Mennucci, B.; Tomasi, J. Towards the elaboration of a QM method to describe molecular solutes under the effect of a very high pressure. *Chem. Phys.* **2008**, *344*, 135−141.
(28) Cammi, R. A new extension of the polarizable continuum model: Toward a quantum chemical description of chemical reactions at extreme high pressure. *J. Comput. Chem.* **2015**, *36*, 2246−2259.
(29) Stauch, T. A mechanochemical model for the simulation of molecules and molecular crystals under hydrostatic pressure. *J. Chem. Phys.* **2020**, *153*, No. 134503.
(30) Scheurer, M.; Dreuw, A.; Epifanovsky, E.; Head-Gordon, M.; Stauch, T. Modeling Molecules under Pressure with Gaussian Potentials. *J. Chem. Theory Comput.* **2021**, *17*, 583−597.
(31) Epifanovsky, E.; Gilbert, A. T.; Feng, X.; Lee, J.; Mao, Y.; Mardirossian, N.; Pokhilko, P.; White, A. F.; Coons, M. P.; Dempwolff, A. L.; et al. Software for the frontiers of quantum chemistry: An overview of developments in the Q-Chem 5 package. *J. Chem. Phys.* **2021**, *155*, No. 084801.
(32) Hsieh, C. M.; Grabbet, B.; Zeller, F.; Benter, S.; Scheele, T.; Sieroka, N.; Neudecker, T.; et al. Can a Finite Chain of Hydrogen Cyanide Molecules Model a Crystal? *ChemPhysChem* **2022**, DOI: 10.1002/cphc.202200414.
(33) Hohenberg, P.; Kohn, W. Inhomogeneous Electron Gas. *Phys. Rev.* **1964**, *136*, No. B864.
(34) Kohn, W.; Sham, L. J. Self-Consistent Equations Including Exchange and Correlation Effects. *Phys. Rev.* **1965**, *140*, No. A1133.
(35) Becke, A. D. Correlation energy of an inhomogeneous electron gas: A coordinate-space model. *J. Chem. Phys.* **1988**, *88*, 1053−1062.
(36) Lee, C.; Yang, W.; Parr, R. G. Development of the Colic-Salvetti correlation-energy formula into a functional of the electron density. *Phys. Rev. B* **1988**, *37*, No. 785.
(37) Becke, A. D. A new mixing of Hartree-Fock and local density-functional theories. *J. Chem. Phys.* **1993**, *98*, 1372−1377.
(38) Hehre, W. J.; Ditchfield, R.; Pople, J. A. Self-Consistent Molecular Orbital Methods. XII. Further Extensions of Gaussian-Type Basis Sets for Use in Molecular Orbital Studies of Organic Molecules. *J. Chem. Phys.* **1972**, *56*, 2257−2261.
(39) Mayer, I. Charge, bond order and valence in the ab initio SCF theory. *Chem. Phys. Lett.* **1983**, *97*, 270−274.
(40) Mayer, I. On Bond Orders and Valences in the Ab initio Quantum Chemical Theory. *Int. J. Quantum Chem.* **1986**, *29*, 73−84.
(41) Bader, R. F. W. Atoms in Molecules. *Acc. Chem. Res.* **1985**, *18*, 9−15.
(42) Lu, T.; Chen, F. Multiwfn: A Multifunctional Wavefunction Analyzer. *J. Comput. Chem.* **2012**, *33*, 580−592.

https://doi.org/10.1021/acsomega.2c05664
ACS Omega 2022, 7, 45208−45214

(43) Kumar, S.; Stauch, T. The activation efficiency of mechanophores can be modulated by adjacent polymer composition. *RSC Adv.* **2021**, *11*, 7391−7396.

https://doi.org/10.1021/acsomega.2c05664
ACS Omega 2022, 7, 45208−45214